Research Article

Ruibo Guo*, Jinchuan Zhang*, Panwang Zhao, and Ziyi Liu

Influence of interbedded rock association and fracture characteristics on gas accumulation in the lower Silurian Shiniulan formation, Northern Guizhou Province

https://doi.org/10.1515/geo-2020-0253
received December 30, 2020; accepted April 26, 2021

Abstract: The northern Guizhou area, located near the southwestern margin of the Yangtze Block, is a promising area for shale gas exploration and development. The Lower Silurian Shiniulan Formation as a new discovery stratum of natural gas marks an exciting breakthrough in natural gas exploration in northern Guizhou area. Based on several field investigations and samples analyses, the lithology and fracture characteristics were systematically analyzed in the lower Shiniulan Formation, and the reservoir specificity and its influence on natural gas accumulation were determined. The characteristics of the relatively fractures and lithology assemblages were identified as key factors controlling the natural gas accumulation. The lower Shiniulan Formation is deposited as calcareous shale and marlstone with frequent centimeter-scale interlayers. This is reflective of a shallow sea shelf strata with decreasing sedimentary rhythm and gradual weakening of sedimentary changes and developed calcareous shale and marlstone with frequent centimeter scale interlayer changes. The gas reservoir is dominated by calcareous mudstone, controlled by the interbedded rock association (calcareous mudstone and limestone), characterized by the raw-storage and the accumulation-reservoir interbedded system. The reservoir is located in the central part of the syncline and is characterized by strong sealing of the stratum, large proportion of free gas, and high abnormal pressure. The Lower Shiniulan Formation is formed between the shale layer with horizontal fractures and dense limestone with underdeveloped fractures. Among them, the shale section generally develops diagenetic shrinkage fractures, which provide good storage space for natural gas and act as the main body of natural gas. The pore sizes in limestone (2.8 nm) are significantly smaller than those in mudstone (7.5 nm), which results in a good capping and preservation of shale gas. This paper reports on results that are of significance for supplementing the theory of unconventional natural gas accumulation and guiding shale gas exploration in similar areas.

Keywords: lithology combination, fracture characteristics, natural gas accumulation, Shiniulan Formation, Guizhou Province

1 Introduction

Along with the rapid development of the economy, the consumption of oil and gas resources is also increasing. Notably, the consumption of oil and gas in China ranks second in the world [1–6]. As a nonrenewable resource, conventional oil and gas resources are gradually declining, while unconventional oil and gas resources gradually increasing in the market share [7,8]. One of the most successful examples of unconventional resource usage is the shale gas revolution in the United States. Unconventional resources with large reservoir potential and low exploration costs have become hot spots for various domestic and global oil companies. To alleviate energy shortages, it is necessary to explore and develop unconventional oil and gas resources, which necessitates targeted research of unconventional resource accumulations [9–14].

The Sichuan Basin is one of high-yield natural gas basins in China. The Silurian Longmaxi and the Upper Ordovician Wufeng Formations are important target layers of high-yield natural gas in the Sichuan Basin and are the main strata in which exploration and development progress have been achieved [15–17,57,65]. Studies of these strata have shown that high yield of shale gas has become

* **Corresponding author: Ruibo Guo,** Guangzhou Marine Geological Survey, China Geological Survey, Guangzhou, Guangdong, China, e-mail: 463786492@qq.com, 3006160043@cugb.edu.cn
* **Corresponding author: Jinchuan Zhang,** School of Energy Resource, China University of Geosciences, Beijing 100083, China; Key Laboratory of Shale Gas Exploration and Evaluation, Ministry of Land and Resources, China University of Geosciences, Beijing 100083, China, e-mail: zhangjc@cugb.edu.cn
Panwang Zhao, Ziyi Liu: School of Energy Resource, China University of Geosciences, Beijing 100083, China

indisputable. Further research confirmed that shales of Wufeng-Longmaxi Formation are the main reservoir of the absorbed and free gas [18–20,58].

The shale gas resource potential survey in Guizhou Province shows that the geological resources of shale gas attain 3.88 trillion m^3. The Wulingshan area experienced many periods of strong tectonic movements, resulting in inadequate oil and gas preservation conditions. Furthermore, it remains unresolved whether the residual syncline is also a potential resource of shale gas. In 2016, AnYe-1 (AY-1) well was drilled on the Anchang slant, which is the first industrial gas well with high yield and within the complex tectonic units in the Upper Yangtze area except the Sichuan Basin [21]. The exploration breakthrough of AY-1 marks the beginning of the unconventional resource exploration and development of 7,800 m^2 residual syncline Wuling Mountain area, which could lead to a breakthrough in oil and gas development in the future [22].

The hydrocarbon was discovered in the Ordovician Baota, the Silurian Wufeng-Ordovician Longmaxi, the Silurian Shiniulan, and the Permian Qixia Formations. The exploration and development of the Ordovician Wufeng – Silurian Longmaxi Formations of shale gas have been studied at an advanced level, while in the Shiniulan Formation high-yield gas has also been discovered and extracted for the first time (Figure 2) [23]. To clarify the enrichment system of high-yield natural gas in the Lower Shiniulan Formation (Fm.), it is necessary to conduct an in-depth study on the main controlling factors of natural gas accumulation such as the lithological composition and fracture distribution characteristics.

The study of the geological background included samples observation and data analysis, characterizations of the lithological composition of the Shiniulan Fm., as well as its corresponding sedimentary environment. Furthermore, combining the observations with the statistics of the developed fracture and reservoir physical properties, the main factors affecting gas accumulation were investigated.

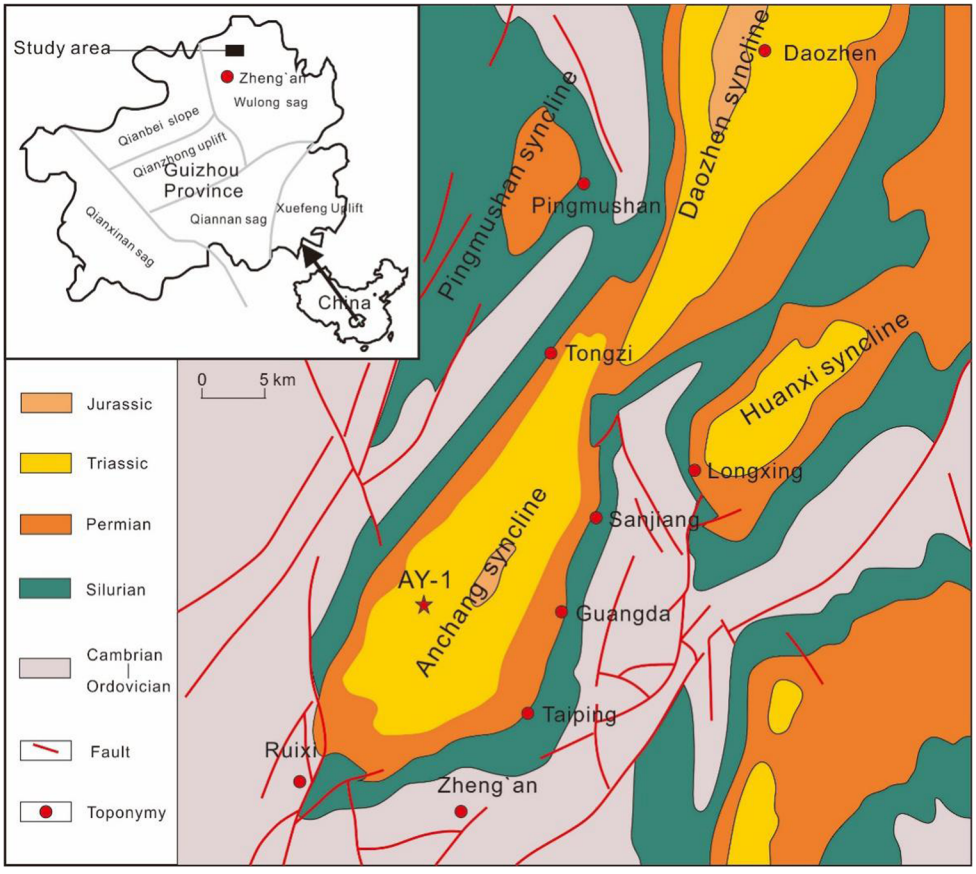

Figure 1: Zheng'an area map of division of the target layer and geological background.

2 Geological setting

Anchang syncline in the northern Guizhou Province is located in the southwestern margin of the Yangtze Block, south of the Sichuan Basin (Figure 1). The syncline core is exposed to the Jurassic-Triassic strata, and the wing is composed of the Silurian-Ordovician strata. The faults of the Cambrian strata in the syncline periphery are relatively well-developed, while the internal faults in the syncline are not developed and there are no typical large faults. The faults in the Longmaxi Formation are generally underdeveloped and the stratum developed is relatively stable. AY-1 well is located in the west wing of the Anchang slant (Figure 1).

This entire area is located on the southern edge of the upper Yangtze plate in the earth structure. In the early Silurian, it experienced extensive transgression deepening of seawater with deposition of black carbonaceous shale, siliceous shale, and rich graptolite [24]. With further sedimentary filling of the Longmaxi Formation and the influence of movement along the Guangxi fault, the relative sea level and sedimentary water depth decreased in deep shelf area, and gradually evolved into shallow shelf facies in the Shiniulan period. These included platform margin slope facies, platform margin shoal facies, and restricted platform facies. At the end of the Shiniulan period, the relative sea level decreased to the lowest point [25]. Deposition of shale, mudstone, siltstone, marl, and limestone followed the decline of the sea level (Figure 2).

The strong movement along the Guangxi fault led to the overall uplift of the block and erosion of the Longmaxi Fm. during the middle-late Silurian. Until the Devonian and Carboniferous, the stratum gradually uplifted and further eroded. The marine-continental transitional facies-limited sea carbonate platform environment is deposited under the stage of transgression from Early to Middle Permian [26]. After the Late Permian, the structure of the Qianzhong uplift and the Upper Yangtze area were completely integrated. The influence of the Qianzhong uplift on the sedimentary environment, basin framework, and tectonic paleogeography ceased. As the Early-Middle Triassic transgression advanced, Anchang syncline reached the carbonate platform environment. Influenced by the Indosinian movement, the uplift of the crust of the area continued steadily during the Early-Middle Triassic and a large-scale regression occurred in the Late Triassic, resulting in the full closure of the Upper Yangtze platform and the complete uplift of the continental crust, ending the period of marine sedimentation in this area [27].

3 Materials and methods

3.1 Sample selection

The studied layer is located in the lower part of the Shiniulan Fm.; it is approximately 100 m thick and mainly composed of centimeter-wide interbedded layers of mudstone and limestone, with (Figure 2). In total, 24 fresh core samples collected at depths of 2,110–2,348 m in the AY-1 well were analyzed, 15 of which were from the Shiniulan Fm., and nine of which were from the Longmaxi Fm. A series of experiments were conducted on these samples to obtain parameters such as porosity, permeability, and mineral composition and to evaluate the characteristics of mudstone samples of the Shiniulan Fm. in the upper Yangtze area [22].

3.2 Observation and statistical classification method for fractures

The observation and statistical analysis of the length, opening, dip, and density of core fractures are fundamental for the study of fracture development and distribution features of cores. Microfractures are small, high-aspect-ratio cracks in rock that result from application of differential stresses [66]. During the identification and observation of core fractures, the core is generally immersed in water so that fractures can be clearly observed before the core surface becomes dry. The reason for this is that there are many microfractures in cores. After the core is immersed in water, and water has completely evaporated from the surface, it still remains within the microfractures; thus, water marks microfractures with the same dip size and helps observing them on the surface of the core.

3.2.1 Statistical analysis and research on the fracture dip of cores

According to the observation statistics and existing research results [60], the variation range of the fracture inclination formed by the stress is divided into four types:

(1) Horizontal joint ($0° \le A \le 15°$): the detachment fracture caused by the shear stress of bedding slip along the layer of the shale under the action of the extension or extrusion structure.
(2) Low-angle oblique crossing joint ($15° < A \le 45°$): mainly a bedding slip joint and a shear joint formed by ductile shearing under regional tectonic stress.

(3) High-angle cutting joints ($45° < A \leq 75°$): High-angle shear joints and tensile shear fractures formed mainly by ductile shearing, often associated with faults or folds.

(4) Vertical joints ($75° < A \leq 90°$): It is mainly a tensile fracture formed under extension. It has a long extension distance on the observed core and does not easily form into a group.

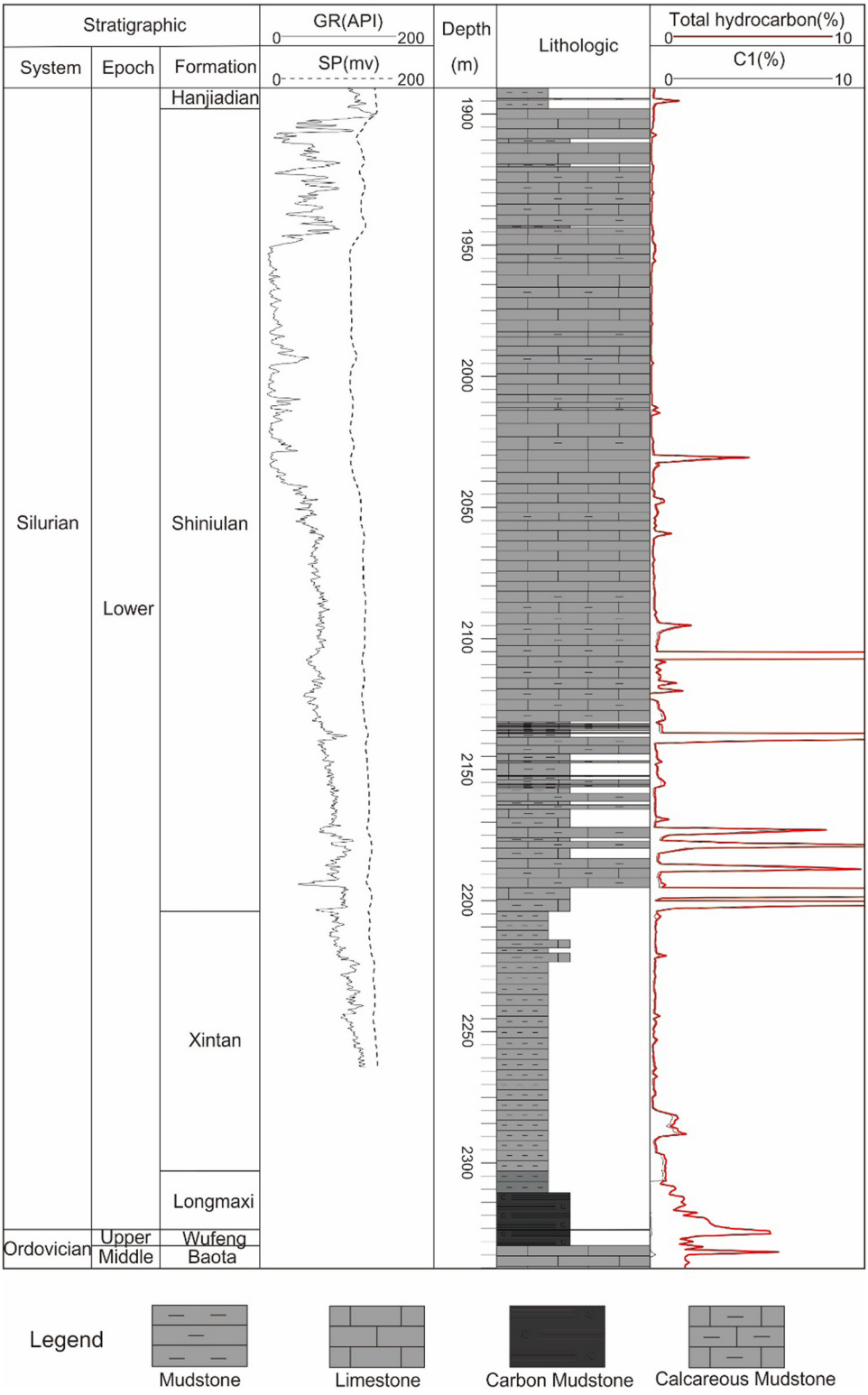

Figure 2: The generalized stratigraphic column and characteristics of logging curves of the upper Ordovician Wufeng-lower Silurian Longmaxi and lower Silurian Shiniulan Formation in the northern Guizhou.

3.2.2 Statistical analysis of the degree of the fracture development in cores

Density of fractures is a significant parameter to describe the degree of fracture development, which can reflect the intensity of fractures. The fracture linear density is one of the most effective parameters indicating the degree of fractures development. It refers to the ratio of the number of fractures intersecting a straight line to the length of the line:

$$D = \frac{N}{H} \tag{1}$$

where N is the total number of fractures observed in the core unit; H is the core length in the unit, m; D is the linear density of fracture, in m^{-1}.

3.3 Petrographic microscope and X-ray diffractometer (XRD) observations of thin sections

Petrographic samples preparation method followed Standard GB/T 15588-2013 and they were examined using a Zeiss Axio Imager Microscope in white and blue incident light. Samples were viewed under oil immersion using a 40 objective, a measuring diaphragm with a 3 mm diameter spot size, and an interference filter with a passband peak of 546 nm [28].

Bulk mineralogy was determined using a D/max-2600 (Rigaku, Japan) X-ray diffractometer (XRD) with Cu-Kα radiation (λ = 1.5418 Å) equipped with automatic divergent and anti-scatter slits, and a secondary graphite monochromator with a scintillation counter [29]. Each XRD pattern was recorded in the 5°–70° 2θ interval, with a step size of 0.02°. Semiquantitative results of the weight percentage of each mineral type were obtained by comparing the results with the available database and corrected for Lorentz polarization [30].

4 Results and discussion

4.1 Lithofacies classification and characteristics

4.1.1 Lithofacies of the Shiniulan Formation

From the bottom to the top, the Shiniulan group sediments generally show characteristics of a shallowing-upward sequence, that is, a deposition sequence from the deep-water continental sediments upward to the shallower-water platform margin reef-shoal facies. The bottom-up lithological response is as follows: the shale content is decreasing upward, the lower and middle segment is mainly composed of thin to thick nodular limestone (Figure 3d), and the upper part contains middle-sized blocky reef limestone, raw limestone, and calcarenite. The sedimentary facies in the platform margin slope are mainly composed of nodular limestone. Most of the nodules in the nodular limestone are bioclastic or argillaceous limestone, and most of the nodules are filled with gray mudstone or argillaceous limestone (Figure 3a). The investigated layer is characterized by limestone interbedded with mudstone and siltstone (Figure 3b). Graptolites, the standardized fossil record at the bottom of the global Tregeci stage [31], are abundant in the lower layer of the section. Shoal facies limestone is mainly developed in the upper Shiniulan Fm. with fossil-rich metazoan (Figure 3c) [23].

It is found that the rock types in the lower of the Shiniulan Fm. show diversity, often including the following: a thin dark-gray or gray layer of calcareous shale, calcium-bearing sandy mudstone, and limestone interbedded with fossils; a thin layer of mudstone irregularly interbedded with limestone; a thick layer of bioclastic limestone irregularly interbedded with mudstone; limestone containing an irregular muddy strip and interbedded with bioclastic limestone, bioclastic limestone, and thick-layered blocky limestone with a thin layer of mudstone; calcareous shale, including fossils of brachiopods, graptolite, and corals.

Different lithologies can be summarized and described bottom-up as follows:

(1) Calcareous mudstone (Calcareous sandy mudstone interbedded with limestone)

Calcareous shale is distributed in the lower part of the Shiniulan Fm., which is common in the continental and transitional red-rock series in sedimentary environment, and is also found in the argillaceous rocks developed in the marine and lagoon sedimentary environment. It mainly consists of dark-gray ~80–90 m thick sandy shale layer, containing fossils in the calcareous mudstone (Figure 4a), which is distributed in the northern part of the Guizhou Province such as Zheng'an and Tongzi counties. Pyrite adheres to the sedimentary surface in granular form reflecting deep-water sedimentary environment with low energy (Figure 4b). The sand content of shale is relatively high and the silty mud analyzed by thin sections is identified to contain low calcium (Figure 4c).

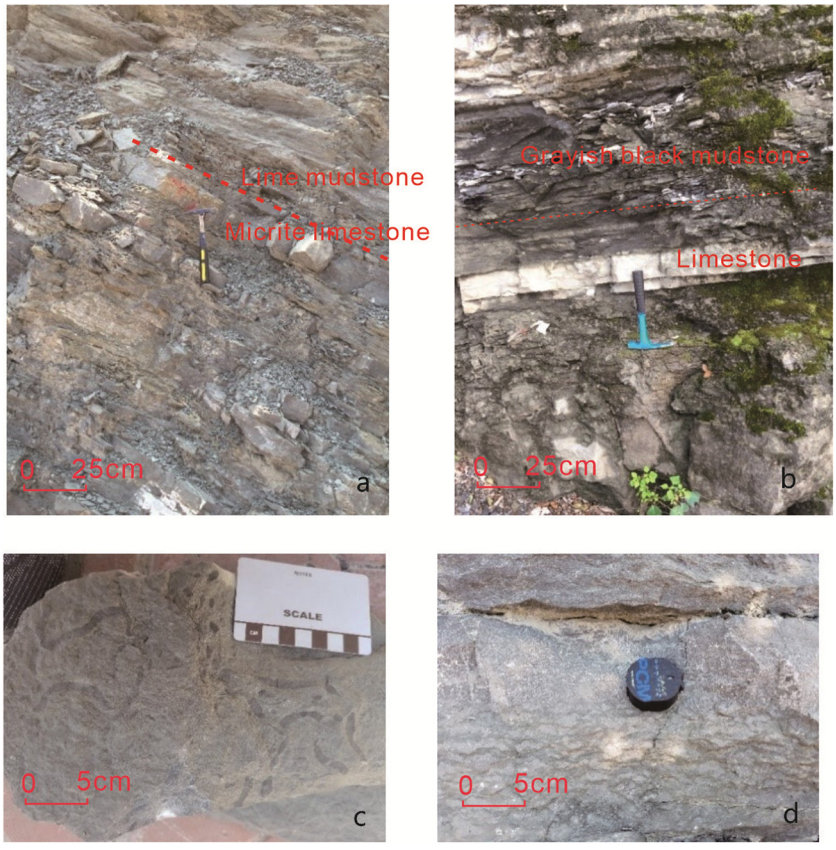

Figure 3: The geological characteristics of Shiniulan Formation. (photos taken from the Majiapo profile). (a) The interbed of thin to medium-layered micrite limestone and thin-layered lime mudstone. (b) The interbed of grayish black mudstone and limestone. (c) Trace fossils in limestone of Shiniulan Formation. (d) Gray medium-thick-layered limestone.

(2) The irregular interbed of mudstone and limestone

The irregularly interbedded layers of mudstone and limestone are located in the middle of the lower Shiniulan Fm. The lithology contains irregularly interbedded layer of thin mudstone and limestone with a thickness of approximately 4–5 m. The overall sequence is inter-layered, layered, and thick, reflecting a relatively low-energy depositional environment.

The shale content gradually decreases upward. The thickness of the layer increases with increasing purity of limestone composition, showing upward-spiraling secondary cyclicity characteristics. In addition, the imperceptible bedding is developed, and the wedge-shaped structure is observed, reflecting a stable, non-agitated high-energy water environment (Figure 5). The rock layer is deformed by the tectonic movement that resulted in development of fractures perpendicular to the sedimentation plane, and mostly filled with calcite. There are some layers along the fracture ruptures containing abundant large crystals of calcite, which may be either externally grown or formed by dissolution and recrystallization of the source rock.

(3) The irregular interbed of mudstone and thick bioclastic limestone

Bioclastic limestone is a product of high-energy sedimentary environment, which is widely distributed in the Shiniulan Fm. Shown in Figure 6, the thick biolimestone and mudstone are irregularly interbedded. The thickness of the limestone layer is ~30–80 cm, and that of the mudstone is generally less than 10 cm. The 1 cm-wide fracture perpendicular to the sedimentary layer is filled with calcite. These settings suggest that water was relatively stable during the limestone formation, changing to an unstable environment during the mudstone formation. The thickness of bioclastic limestone generally increases, owing to the transformation of sedimentary environment from a relatively low-energy to a high-energy environment.

(4) The interbed of limestone with an irregular mud strip and thick bioclastic limestone

The interbedded layers of irregular muddy strips and bioclastic limestones within a thick limestone are mainly

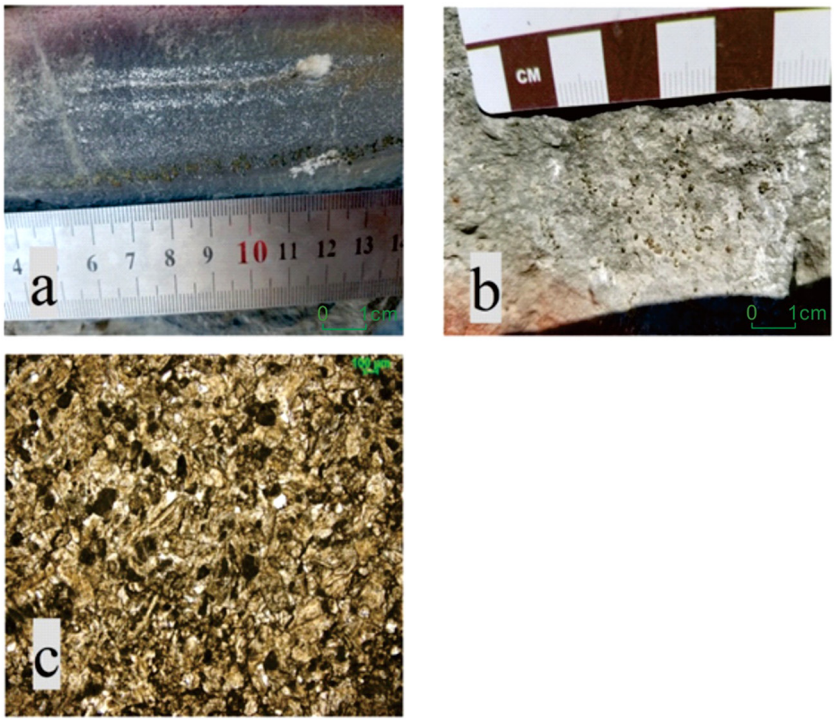

Figure 4: The characteristics of calcareous mudstone and thin section of samples observed under microscope. (a) Photos of the core of AY-1 well whose lithology is calcareous mudstone; (b) visible pyrite crystals; (c) Slice observation shows that the structure is argillaceous and silty, and the rock is mainly composed of argillaceous, followed by silty.

located in the upper middle part of the Shiniulan Fm. with a total thickness of the layer ~14 m and an interbed limestone thickness of ~20–40 cm. The muddy strips are well-developed within the lower part that contains thick interbedded layers of bio-limestone and mudstone. The thickness of the bioclastic limestone generally increases. The mudstone becomes interbedded with limestone and mudstone, reflecting that the sedimentary environment is gradually transformed from a relatively low-energy to a more energy-efficient environment. The profile observation shows that the shale content is gradually reducing upward. The thickness of the layer increases with the purification of the limestone composition, showing shallower secondary cycle characteristics (Figure 7).

(5) The interbed of thick limestone and calcareous mudstone

The interbedded layer of thick limestone and mudstone is located in the upper part of the Lower Shiniulan Fm., with a profile thickness of ~11 m; the thickness of the limestone with a massive structure is 30–80 cm, and the thickness of the mudstone in thick interbedded layers of limestone is less than 1 cm. The layer of mudstone is well-developed, with a ~40 cm thickness of individual layers. This layer contains developed fractures that are almost perpendicular to the bedding plane, most of which are not filled or contain only a small amount of calcite, indicating a relatively low-energy sedimentary environment of a shallow shelf (Figure 8).

4.1.2 Lithofacies association characteristics and corresponding sedimentary environment

Following the detailed description of the lithological associations in the lower Shiniulan Fm., sedimentary evolution of this layer can be inferred. The Shiniulan Fm. in the study area contains diverse lithology. There are few studies on the gradual change of lithofacies and biofacies and the controlling factors of the sedimentary environment [32]. At present, it is clear that the lower Shiniulan Fm. belongs to transitional sedimentary facies of progressively shallower clear seawater, which can be classified as the neritic shelf [31,33–36]. The sedimentary characteristics of a sharp decline in the sea level continued from the late Longmaxi Fm. stage into the mainly shallow shelf sea of the Shiniulan Fm. In the early stage of sedimentation, terrigenous clastic particles were

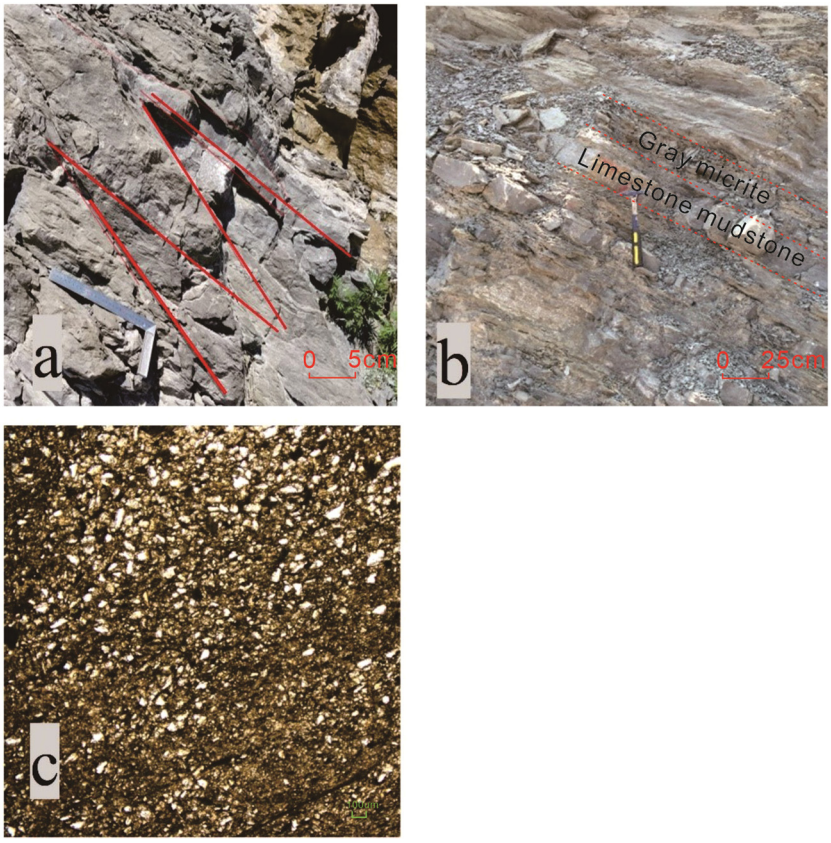

Figure 5: The characteristics of calcareous mudstone and thin section of samples observed under microscope. (a) Wedge-shaped cross bedding; (b) thin interbed of gray micrite and limestone mudstone; (c) silty sandy argillaceous structure; this sample is mainly composed of calcite, followed by argillaceous, quartz, and muddy sandy powder-fine grain (2,130 m).

abundant. In particular, the microscopic carbonate minerals and mudstones contained a large amount of terrigenous clastic quartz depositing mixed sedimentary layers with thin interbeds of mudstone and limestone under the tidal influence and local sea level rise. Following the sea level rise, the input of terrigenous detritus gradually decreased and the water cleared, leading to an increasing thickness of the limestone deposits. By the time of the Shiniulan Fm. deposition, the supply of terrigenous clastic material was highly reduced. The water became very clear and a shoal-bar developed, as inferred by the sedimentary deposits of bioclastic limestone interbedded with a small amount of sandstone-limestone.

As reflected in the facies, the sedimentation reached a turning point from the clastic facies of the Longmaxi Fm. to the reef (shoal) facies of the overburden Shiniulan Fm. The lower Shiniulan Formation in the north of Guizhou shows characteristics of a significant mixing during accumulation. For example, terrigenous detritus, which mainly comes from the central Guizhou uplift in the south, can be found deposited in the limestone. Different depths of sedimentary water and hydrodynamic forces can also lead to differences in the lithofacies [31]. Near-shore facies experienced more intensive hydrodynamics, which led to deposition of a granular limestone. Terrigenous detrital material and bioclastics are mostly coarse-grained. In contrast, far-shore facies experienced less hydrodynamics, leading to deposition of carbonate particles, mostly silt and mud. Terrestrial debris was effectively transformed into mud-grade particles after long-distance handling [32]. The resulting lithology comprises an interbed layer of thin gray limestone and argillaceous limestone. The thickness of the argillaceous limestone is increasing upward. There is no large fault zone in the study area within the stable internal structure. The stratum thickness of the lower Shiniulan Fm. is widely and continuously distributed from south to north.

4.2 Fracture distribution characteristics

Fractures are an important part of the pore composition of mudstones. Fractures not only provide space for gas storage, but also serve as a conduit for gas circulation [44].

Figure 6: The characteristics of thick limestone and mudstone and thin section of samples observed under microscope. (a) Irregular interbed of thick limestone and mudstone. (b) Thick limestone. (c) The siliceous structure contains siliceous and Bioclastic sparry. The sample is mainly composed of calcite, followed by quartz and other minerals. The stratification can be clearly seen under the microscope.

The formation of fractures is related to tectonic movements such as faults and folds, but also to non-structural causes such as dehydration of clay minerals. Lithology and mineral composition are the main factors controlling the degree of development of fractures [37–40]. The mineral composition of shale is complex, containing detrital and

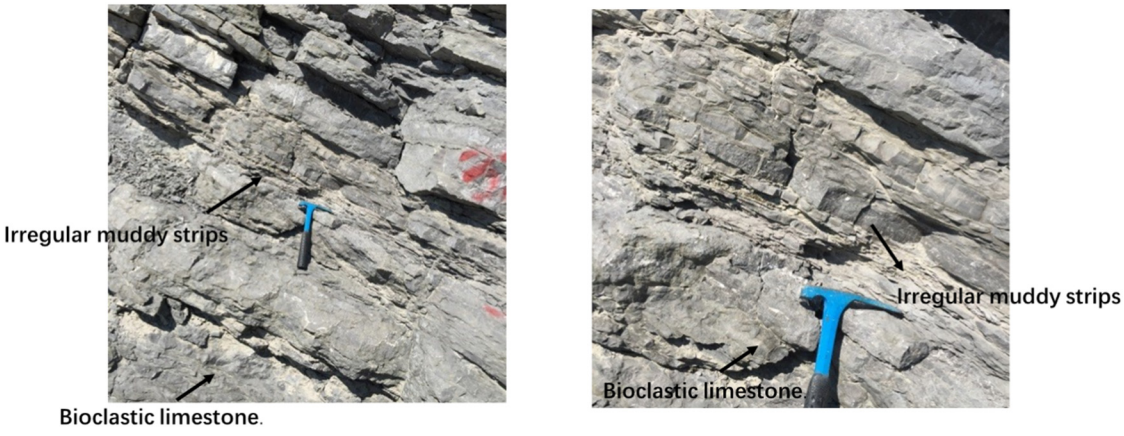

Figure 7: The interbed limestone and irregular mudstone and bioclastic limestone.

Figure 8: The interbed thick limestone and calcareous mudstone (Majiapo profile).

authigenic minerals such as quartz, calcite, feldspar, and mica in addition to clay minerals such as illite, montmorillonite, and kaolinite (Table 1). The content of quartz can be very high, nearly matching that of clay composition, often appearing in the form of lamina. Shales with high content of organic matter and quartz are brittle, susceptible to formation of natural fractures induced under external forces, which is beneficial for accumulation of natural gas [41,42]. The contents of organic carbon and quartz are important factors affecting the development of fractures. Nelson [43] argues that in addition to quartz, feldspar and dolomite can also act as brittle components in shale.

Fracture identification and characterization methods mainly include geological and petrological methods, drilling and logging, as well as the method of the fracture production dynamic data analysis [67]. The observation and statistical analysis of the length, opening, dip, and density of fractures of samples are the basic data for the study of the degree of development and distribution of fractures. After observing the core slices under SEM field emission scanning electron microscope (Figure 9), it is found that fractures are mainly developed at the edge of minerals and the edge of organic matter bands, and there are also some dissolution fractures. There are two main reasons for the formation of contraction joints: (1) Shrinkage fracture caused by dehydration of clay minerals in diagenesis; (2) Mineral phase transformation. Due to the uneven stress of minerals with different hardness, microfractures are formed on the side of smaller hardness.

In addition, through the observation and measurement of the outcrop in the Lower Silurian Shiniulan Fm. (Figure 10), it was found that the structural fractures included tensile fractures and shear fractures. The shear fractures have a deep cutting-bed section, stable occurrence, and further extension, with fracture angles in the range of 45–90°. Tension fractures often appear in parallel and in groups, with obvious directionality and regular distribution. Structural fractures are generally filled with secondary materials such as calcite and are produced in the areas in which the deformation is severe, or the faults are well-developed (Figure 11).

The finer the mineral particles, the more favorable the fractures development [63]. On the contrary, the thicker the mineral particles, the less fractures developed. The development of fractures is common in the area with lithological changes. Diagenetic shrinkage microfractures are commonly found in mudstones and are rare in carbonate rocks in the lower Shiniulan Fm. (Figure 12). The diagenetic shrinkage microfractures in the mudstone are always developed due to dry shrinkage,

Table 1: The mineral constituent of mudstone core samples in AY-1 well

No. sample	Depth (m)	Mineral composition (%)			
		Quartz	Feldspar	Calcite	Clay
1	2,110	21	14	35	22
2	2,117	29	13	31	25
3	2,119	31	11	30	27
4	2,122	33	16	35	15
5	2,131	28	18	36	17
6	2,142	43	19	20	17
7	2,146	42	15	25	17
8	2,148	43	15	22	19
9	2,151	41	17	30	11
10	2,152	16	12	65	7

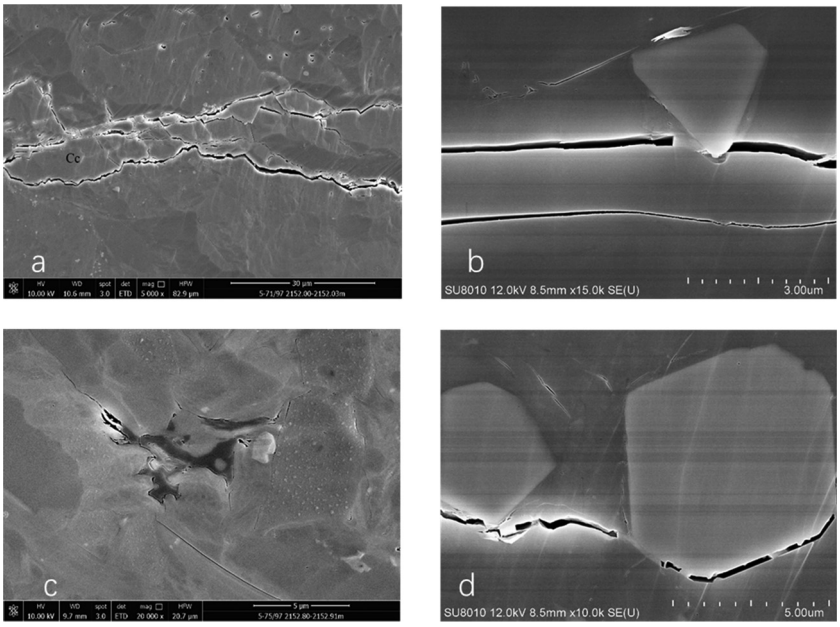

Figure 9: Microscopic characteristics of Shiniulan and Fm. mudstone fractures. (a) Microfractures are formed from the dissolution of calcite. (b) Microfractures are formed from diagenetic shrinkage. (c) Microfractures are formed around development of organic matter strips. (d) Microfractures are formed around development of pyrite skeleton minerals.

dehydration, mineral phase transformation, or thermal contraction.

The systematic observation and statistical analysis of the fractures in the 51.5 m core from the Shiniulan Fm. have been completed, yielding a total of 1,176 observed fractures.

Through the statistical analysis of the fracture length, we come to the conclusion that the fractures of the Shiniulan Fm. are mainly shrinkage fractures resulting from diagenesis, and a small number of them are high-angle shear fractures. The aperture of shrinkage fractures resulting from diagenesis, which are parallel to the bedding plane, are all less than 0.2 mm, whereas the apertures of the high-angle shear fractures are in the range of 0.2–0.5 mm. In the Shiniulan Fm., the fractures are generally long, with the maximum observed length of ~50 cm.

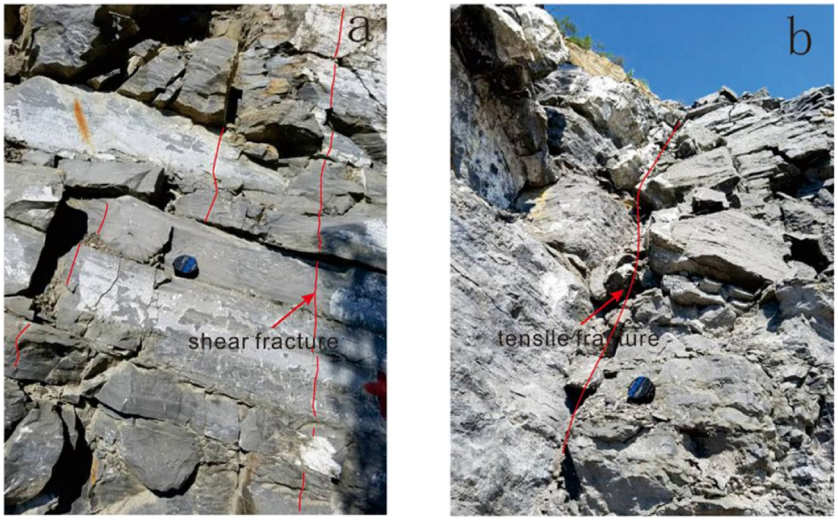

Figure 10: Photos about development of fractures at the Outcrop. (a) The thick-bedded limestone of the Shiniulan Fm. develops shear fractures, which are filled with calcite. (b) tensile fractures are developed in the interlayer formed by mudstone and the middle-thick limestone of the Shiniulan Fm., which are filled with a large amount of calcite.

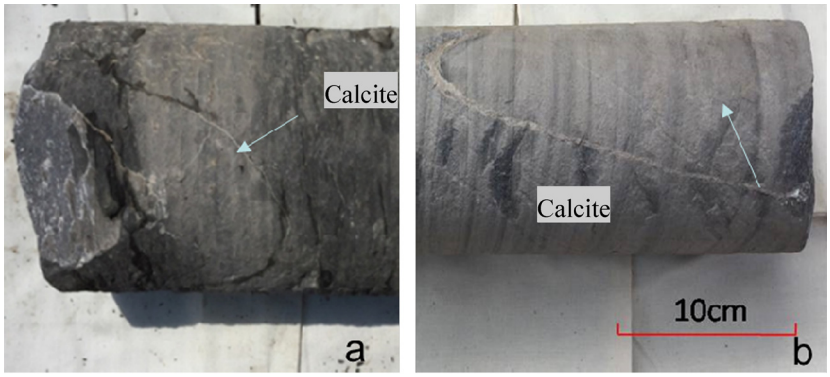

Figure 11: Limestone developed high-angle shearing fractures and calcite filling in core samples.

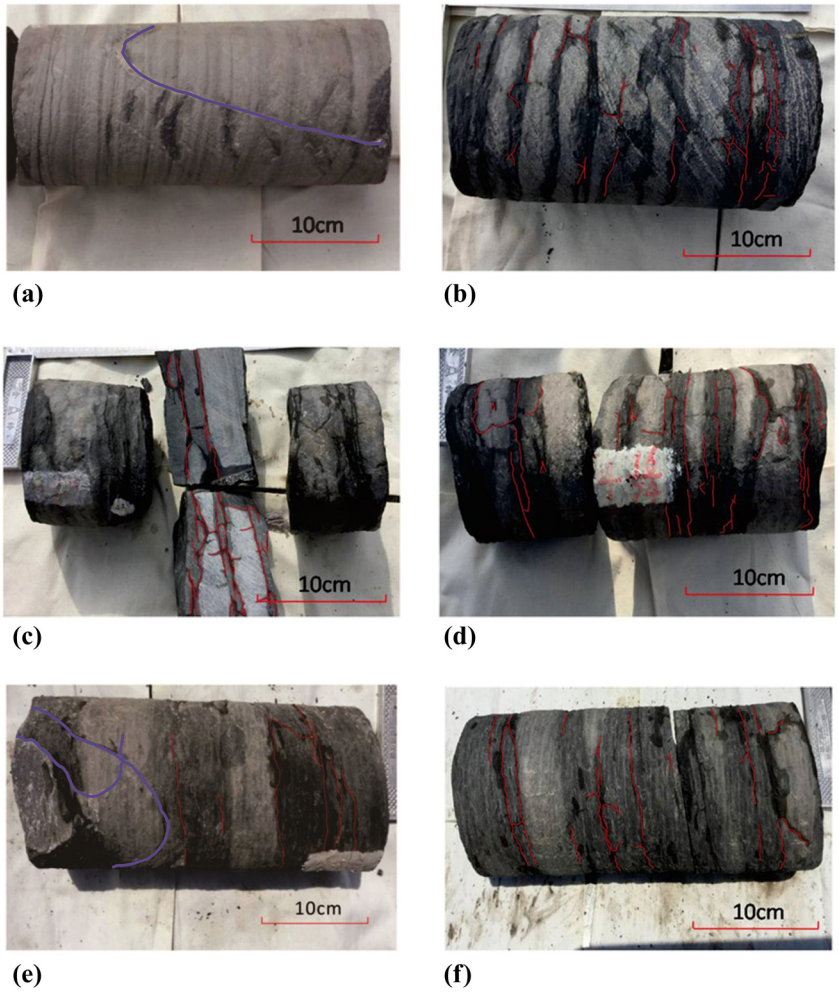

Figure 12: Photos about the core fractures of Shiniulan Formation. (a) Depth: 2107.20–2108.08 m high-angle shear fractures filled with calcite; (b) depth: 2107.20–2108.08 m shrinkage result from diagenesis; (c) depth: 2111.41–2112.15 m shrinkage fractures result from diagenesis; (d) depth: 2125.61–2126.44 m shrinkage fractures result from diagenesis; (e) depth: 2137.80–2138.75 m multi-stage structural fractures and shrinkage fractures result from diagenesis; (f) depth: 2151.96–2152.91 m shrinkage fractures result from diagenesis.

Those fracture apertures cannot be used to predict the original fracture apertures *in situ* due to the large overburden stresses induced by compaction of the overlying strata [64].

According to the statistical results of the proportion of a fracture dip formed by the stress, the diagenetic contraction fractures are dominant, while the high-angle shear fractures account for 60% of the stress fracturing (Table 2). The dip angle of the fractures caused by the stress can indirectly reflect the strength and type of tectonic activity and the corresponding relationship between the dip angle of the fractures and the tectonic action. The AY-1 well is located in the southern section of the west wing of the Anchang syncline in the Wuling fold area, where the structure is relatively stable, leading to the high-angle shearing joint that is dominant in the stress fracture of the core.

The linear density of fractures (Figure 13) is used to characterize the development of core fractures. The statistical results are as follows:

The linear density of fractures (Figure 11) is used to characterize the development of core fractures. The statistical results are as follows:

Depth: 2039.19–2040.90 m. The lithology comprises a thin layer of mudstone with biolithic limestone, with high-angle shearing fractures and calcite filling. The average linear density of fractures is 7 m^{-1}, and the fracture is not developed.

Depth: 2107.20–2125.00 m. The lithology contains an irregularly interbedded layer of limestone and mudstone, which are developed without filling minerals. The average linear density of fractures is 31 m^{-1}, with microfractures present.

Depth: 2125.00–2157.00 m. The lithology contains a regularly interbedded layer of limestone and mudstone. The shrinkage fractures that result from diagenesis are well-developed without filling minerals. The average linear density of fractures is 20 m^{-1}, with well-developed microfractures.

Through the statistical analysis of core fractures, shrinkage fractures resulting from diagenesis in the Shiniulan Fm. mudstone are well-developed, while the structural fractures formed due to stress are rare. The microfractures that developed in mudstone are mainly caused by mineral phase transformation or shrinkage caused by water loss during diagenesis and consolidation and had no link with the sediment structural features.

Table 2: Statistics for angle of core fractures caused by stress

Formation	Proportion of dip angle (%)			
	$0° \le A \le 15°$	$15° < A \le 45°$	$45° < A \le 75°$	$75° < A \le 90°$
Shiniulan	0	20	60	20

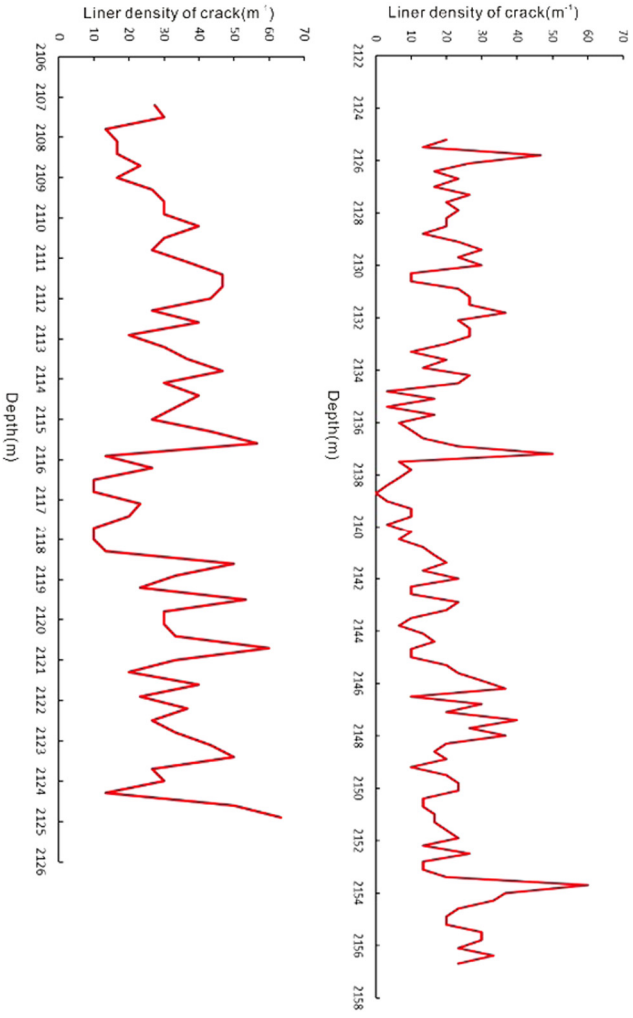

Figure 13: The variation trend of linear density of fractures with depths (left). The average linear density of the fracture is 31 m^{-1}, and the microfractures are well-developed (right). The average linear density of the fracture is 20 m^{-1}, and the microfractures are well-developed.

Moreover, most of the microfractures in the Shiniulan Fm. shale are not filled with minerals, while most of the microfractures developed in the limestone are filled with calcite. Because of calcite deposition in limestone fractures, the fracture density in limestone is lower compared to mudstone (Figure 14).

The logging data and micro-resistivity image logging information show that most of the layers in Shiniulan Fm. have good stratigraphic stratification and well-developed horizontal bedding, with no obvious structural fractures (Figure 13). Because of the frequent interbeds of limestone and mudstone in the Shiniulan Fm., the layers are also not susceptible to the development of dissolution

holes, and no dissolution fractures in limestone were found by micro-resistivity image logging.

There are four depth segments corresponding to the high abnormal hydrocarbon value of gas in Shiniulan Fm., namely, 2,105–2,110 m, 2,132–2,142 m, 2,170–2,180 m, and 2,183–2,203 m (Figure 15). GR is usually used to characterize the radioactive content in the strata and the GR value of mudstone is relatively high. The position of the high GR value corresponds to the strong oil and gas signal, where the corresponding DEN value is also slightly increased, indicating that a large amount of gas is stored in the mudstone.

These four depth ranges show the presence of structural fractures with different angles and extensions, as seen in the high values near the site of structural fractures recorded by micro-resistivity scanning imaging logging. Thus, a small number of high-angle fractures and vertical fractures (angle is between 60° and 90°) are scattered and developed within the 2,158–2,210 m segment.

The horizontal fractures are developed within mudstone. According to the desorption data and gas anomaly, it can be seen that the high gas content is closely related to the developed horizontal fractures within mudstone [44–46]. The density of fractures and the dispersion of strikes are the main geological factors controlling the production capacity of natural gas [47]. The more fractures, the more dispersed the strike, and the higher the gas production [61]. The proper development of natural fractures that are open and mutually perpendicular can increase natural gas reservoir production [48].

4.3 Influence of reservoir specificity on natural gas accumulation

The centimeter-sized interbedded lithologic assemblages and the microfractures that are particularly abundant in the lower Shiniulan Fm. are the main factors controlling the natural gas accumulation in AY-1 Well.

These frequently interbedded lithologic assemblages are characteristic of the natural gas reservoir of Shiniulan Fm. and a key factor controlling its accumulation. The sedimentary environment of the lower of Shiniulan Fm.

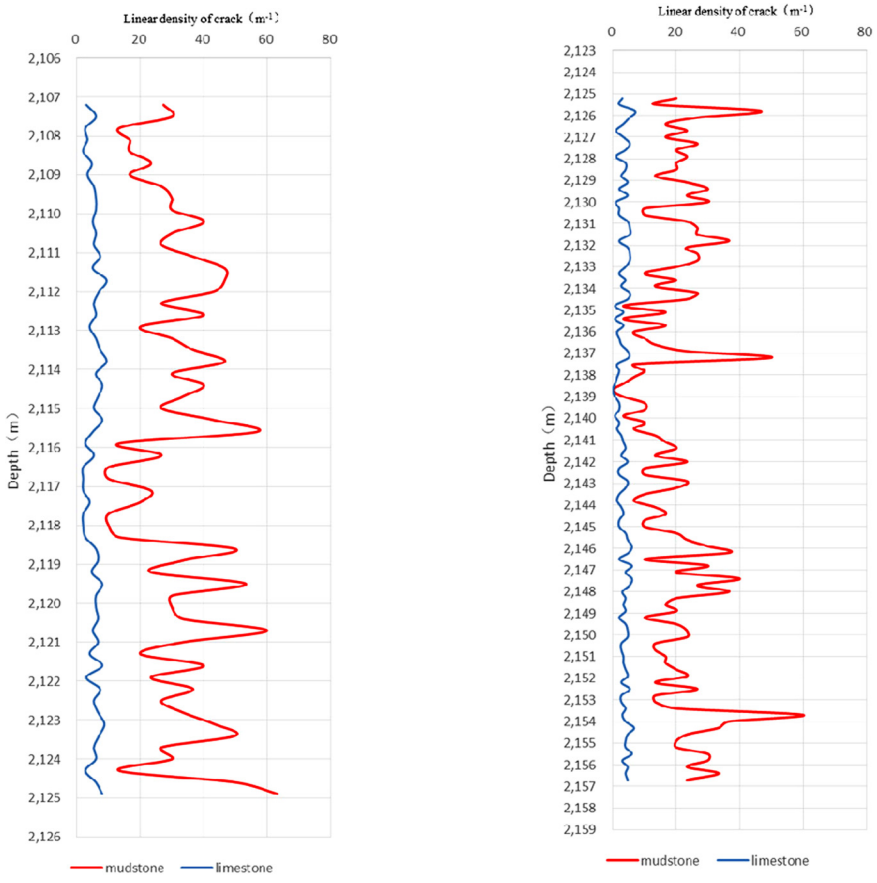

Figure 14: Comparison of mudstone and limestone fractures of Shiniulan Formation.

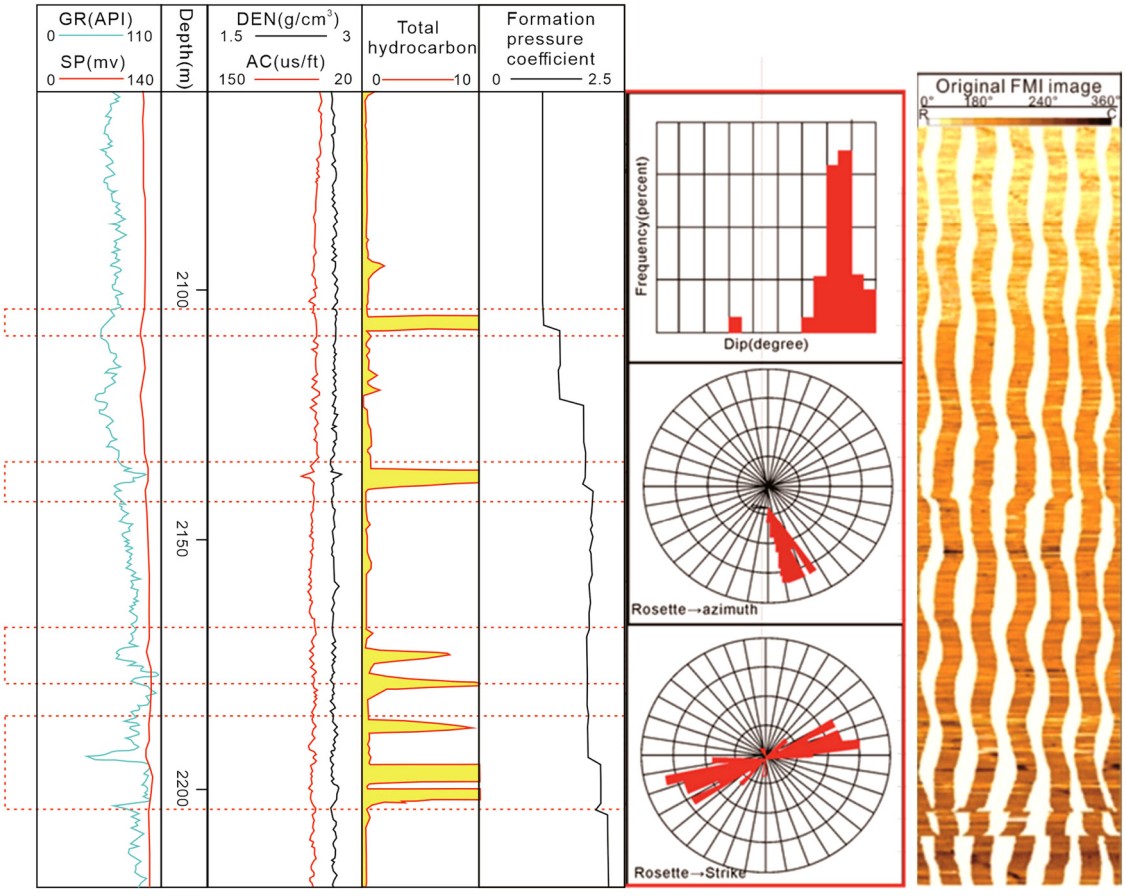

Figure 15: The Fullbore Formation Microimager and logging curve of the Shiniulan Formation.

is of a neritic shelf. The rhythmic change in sedimentary environment forms a special centimeter-sized lithologic combination of calcareous shale and marlstone. This interbedding mode with high sealing property enables the natural gas generated in the Shiniulan Fm. to be preserved to the maximum extent, which leads to abnormally high pressure.

It is evident from the photographs of the profile and core samples that the thin layers of calcareous mudstone and limestone are frequently interbedded with an interval that is less than 1 cm (Figure 16a and c). Mudstone and limestone are irregularly interbedded with syn-deformation features generally developed in the layers (Figure 14b and d).

According to the statistical thickness of core samples (Table 3), the mudstone thickness accounted for 62.7%. It indicates that the lower Shiniulan Fm. is not a simple carbonate reservoir, but a lime-mudstone reservoir with limestone inclusions.

According to the summary of the fracture distribution characteristics, the fractures are mainly developed in the shale, and the limestone fractures are underdeveloped with a small pore diameter. The degree of fracture development in the lower Shiniulan Fm. shows a correlation relationship with the gas content, and the more natural gas is accumulated in the part where fractures are developed. The shale layer with more developed fractures is the reservoir of natural gas, and the denser limestone acts as a caprock, which effectively blocks the escape of the natural gas.

The core samples of the lower part of the Shiniulan Fm. show that the mudstone and limestone are frequently interbedded, with the interbed thickness of individual intervals as low as centimeters. The average porosity is 1.26%, and the permeability is less than 0.01×10^{-3} μm^2, which characterizes a tight reservoir [21]. The pore size in the limestone (2.8 nm) is significantly lower than that in the mudstone (7.5 nm). This lithological arrangement maximizes the preservation of natural gas [49,50], and the statistical and imaging logs of core fractures show that there are fewer developmental fractures in the limestone section, most of which are filled with calcite, which further proves the storability of limestone and control of the loss of natural gas [53,54]. The top-developed thick

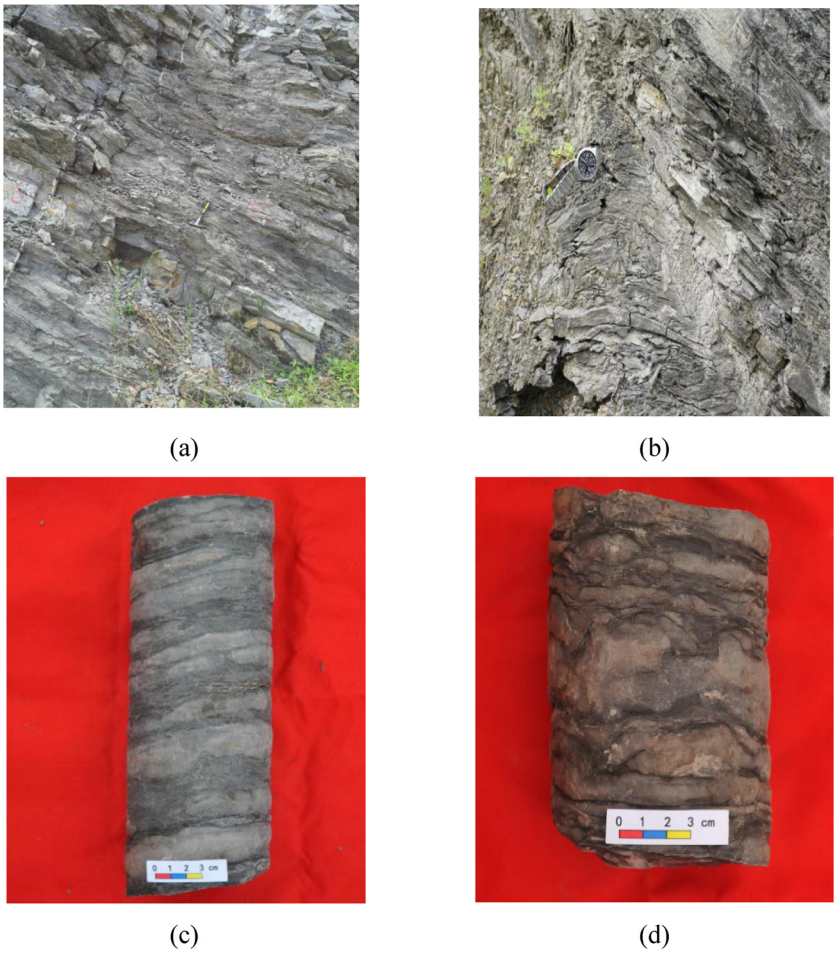

Figure 16: The photos of the Lower Shiniulan Formation in Majiapo profile and core samples from AY-1. (a) Thin mudstone and marlstone are frequently interbedded in profile. (b) Contemporaneous deformation structures which are observed in profile. (c) The interbed of thin mudstone and limestone. (d) Mudstone and limestone irregular interbedded layers with contemporaneous deformation structures.

bioclastic limestone is an available cap rock to prevent the leakage of shale gas (Figure 17). The locally developed high-angle fractures resulted in a short-distance upward migration of natural gas and high-yield gas accumulation where the horizontal fractures developed and the high-angle fractures are lacking [51,52]. The logging data also show that the formation pressure coefficient of the lower part of the Shiniulan Fm. is more than 1.8, which characterizes an overpressurized gas reservoir [59]. The formation of this overpressure is closely related to properties of clay-shales to sustain high stress and to the sealing of the gas reservoir [62], confirming that the Shiniulan Fm. has good sealing properties, which lead to an effective preservation of the natural gas stored in it [55,56].

Therefore, the lithological assemblage and fracture characteristics of this frequent interlayer which are characteristic of the lower Shiniulan Formation shale gas reservoir act as the key factor controlling the gas accumulation (Figure 15). The sedimentary evolution and structure of the Shiniulan Fm. control its stratigraphic development and hydrocarbon generation within it. The rhythmic change in the sedimentary environment may be the key factor that led to the formation of frequently interbedded calcareous shale and limestone. The structure of the region is stable without large fault zones, which ensures the continuous hydrocarbon generation and preservation in the Shiniulan Fm. despite the complex tectonic and geological past. The adsorption capacity of natural gas is weak because of the gray matter in calcareous shale, with most natural gas accumulating in free state in pores and fractures. The small faults developed in the area promote the production of local microfractures, resulting in the accumulation of natural gas. The thick limestone overlying the Shiniulan Fm. and the interbedded rock association (calcareous mudstone and

Table 3: Statistics table of thickness of mudstone and limestone samples (AY-1)

Depth (m)	The thickness of limestone (cm)	The thickness of mudstone (cm)	The percentage of mudstone (%)	Depth (m)	The thickness of limestone (cm)	The thickness of mudstone (cm)	The percentage of mudstone (%)
2107.20–2108.08	41.7	46.3	52.6	2132.69–2133.54	38.3	46.7	54.9
2108.08–2108.96	73	15	17.0	2133.54–2134.26	18.5	53.5	74.3
2108.96–2109.59	53.6	9.4	14.9	2134.26–2135.06	31	49	61.2
2109.59–2110.57	49	49	50.0	2135.06–2136.02	29.5	66.5	69.3
2110.57–2111.44	32	55	63.2	2136.02–2136.99	33	64	66.0
2111.44–2112.15	35.5	35.5	50.0	2136.99–2137.80	34.5	46.5	57.4
2112.15–2113.11	34.8	61.2	63.8	2137.80–2138.75	31.5	63.5	66.8
2113.11–2113.96	45.7	39.3	46.2	2138.75–2139.55	26.5	53.5	66.9
2113.96–2114.91	48.4	46.6	49.1	2139.55–2139.88	21.4	11.6	35.2
2114.91–2115.70	44.2	34.8	44.1	2139.88–2140.76	22.5	65.5	74.4
2115.70–2116.61	35.2	55.8	61.3	2140.76–2141.72	19	77	80.2
2116.61–2117.50	36.5	52.5	59.0	2141.72–2142.58	28	58	67.4
2117.50–2118.55	32.2	72.8	69.3	2142.58–2143.47	26	63	70.8
2118.55–2119.45	49	41	45.6	2143.47–2144.40	22.9	70.1	75.4
2119.45–2120.25	32.7	47.3	59.1	2144.40–2145.33	25.5	67.5	72.6
2120.25–2121.03	40.7	37.3	47.8	2145.33–2146.17	31.1	52.9	63.0
2121.03–2121.89	46.1	39.9	46.4	2146.17–2146.99	29.8	52.2	63.7
2121.89–2122.73	29.4	54.6	65.0	2146.99–2147.91	32.6	59.4	64.6
2122.73–2123.74	42.7	58.3	57.7	2147.91–2148.64	18.2	54.8	75.1
2123.74–2124.68	44.2	49.8	53.0	2148.64–2149.48	20.4	63.6	75.7
2124.68–2125.61	42.7	50.3	54.1	2149.48–2150.49	32.6	68.4	67.7
2125.61–2126.44	38.5	44.5	53.6	2150.49–2151.17	13.8	54.2	79.7
2126.44–2127.36	33.4	58.6	63.7	2151.17–2151.95	15.6	62.4	80.0
2127.36–2128.26	33.5	56.5	62.8	2151.95–2152.91	16	80	83.3
2128.26–2129.19	44.5	48.5	52.2	2152.91–2153.82	5	86	94.5
2129.19–2130.07	29.3	58.7	66.7	2153.82–2154.67	11	74	87.1
2130.07–2131.15	34	74	68.5	2154.67–2155.53	24	62	72.1
2131.15–2131.86	21.7	49.3	69.4	2155.53–2156.43	16	74	82.2
2131.86–2132.69	25.6	57.4	69.2	2156.43–2157.00	11	46	80.7

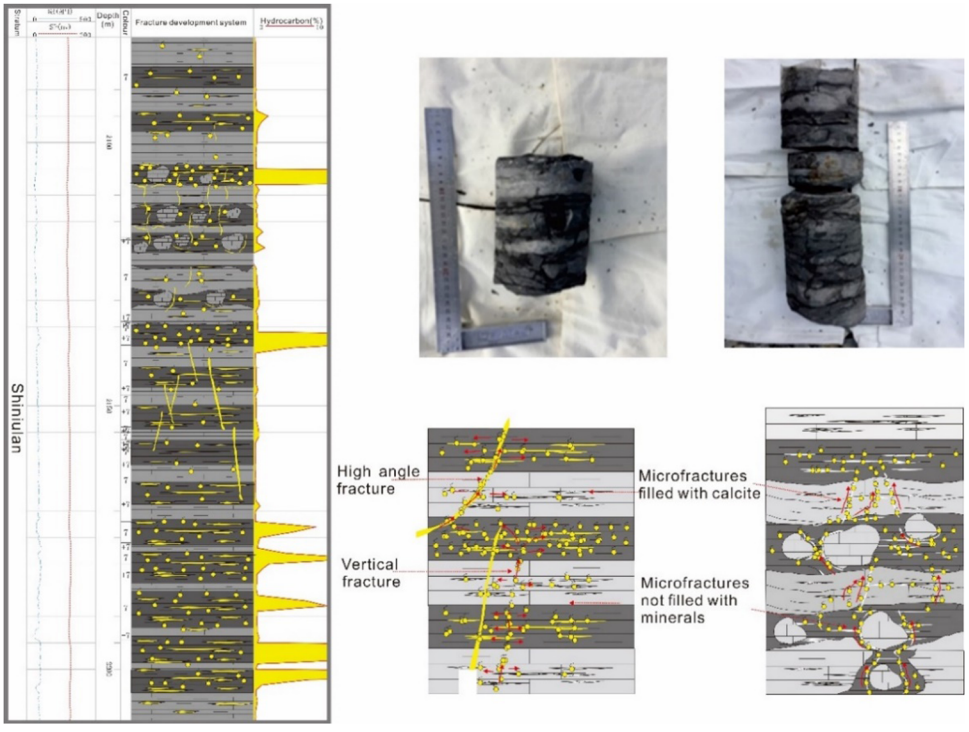

Figure 17: Fractures development pattern of the Shiniulan Formation core samples.

limestone) block the dispersion of natural gas, giving rise to the sealing of the Shiniulan Fm. and to the high pressure formation, which provides a suitable environment for the preservation of natural gas.

5 Conclusions

1. The sedimentary environment of the lower Shiniulan Fm. is transitional leading to development of sedimentary facies that gradually become shallower, while the water body becomes clearer. From the perspective of lithofacies, the dark-gray to gray thin calcareous mudstone and argillaceous limestone are interbedded, with the argillaceous limestone gradually increasing upward.
2. Microfractures developed in mudstone act as space for gas storage. A small number of unfilled high-angle fractures also developed throughout the sequence, further improving the gas storage capacity of the reservoir. Limestone sections have fewer fractures, and most of them are filled with calcite, which further enhances the sealing ability of limestone.
3. The relatively stable geological structure and the rhythmic changes in the sedimentary environment are key factors that control the high-yield gas reservoir in the lower part of the Shiniulan Fm. The layer is characterized by frequently interbedded (centimeter-sized) interlayers, strong sealability, and high pressure. The characteristics of mudstone fractures in the Shiniulan Fm. and the lithological assemblage make it a uniquely suited reservoir to achieve high gas production. Department of oil and gas exploration provides more effective practical significance.

Acknowledgements: The authors are grateful for the valuable comments and suggestions from Prof. Xuan Tang, managing editor Dr. Jan Barabach, other editors, and anonymous reviewers.

Funding information: This study was funded by the Guangdong Major project of Basic and Applied Basic Research (No.2020B0301030003).the Excellent Supervisor Funded Program of the Ministry of Education (grant number 2-9-2017-317), Gas accumulation model of well AY-1 in Guizhou Province, and Evaluation and parameter optimization of shale gas resources in typical areas of South China.

Author contributions: Ruibo Guo: Conceptualization, Methodology, Software, Writing - original draft, Data curation, Writing - review & editing. Jinchuan Zhang: Project administration, Supervision. Panwang Zhao: Methodology, Formal analysis, Resources. Ziyi Liu: Investigation, Visualization, Software.

Conflict of interest: The authors declare that they have no known competing financial interests or personal relationships that could have appeared to influence the work reported in this paper.

References

[1] Jia CZ, Zheng M, Zhang YF. Unconventional hydrocarbon resources in China and the prospect of exploration and development. Pet Exp Dev. 2012;39(2):129–36.
[2] Zou CN, Dong DZ, Wang SJ, Li JZ, Li XJ, Wang YM, et al. Geological characteristics and resource potential of shale gas in China. Pet Exp Dev. 2010;37:641–53.
[3] Martineau DF, Zheng H, Peng Y, Tang J, Shufan LU, Luo X, et al. History of the Newark East field and the Barnett Shale as a gas reservoir. AAPG Bull. 2007;4(4):399–403.
[4] Bowker KA, Ma Y, Zhong N, Yao L, Sun M, Zhang L, et al. Barnett Shale gas production, Fort Worth Basin: issues and discussion. AAPG Bull. 2007;91(4):523–33.
[5] Zhang JC, Nie HK, Xu B, Jiang SL, Zhang PX, Wang ZY. Geological condition of shale gas accumulation in Sichuan Basin. Nat Gas Ind. 2008;28:151–6.
[6] Pollastro RM, Jarvie DM, Hill RJ, Adams CW, Wang E, Liu G, et al. Geologic framework of the Mississippian Barnett Shale, Barnett-Paleozoic total petroleum system, Bend arch-Fort Worth Basin, Texas. AAPG Bull. 2007;91(4):405–36.
[7] U.S. Crude oil and natural gas proved reserves. Washington, USA: Energy Information Administration (EIA); Year-End 2017.
[8] British Petroleum Company. BP statistical review of world energy. London: British Petroleum Company, 2011; 2011.
[9] Hao F, Zou H, Lu Y, Ma Y, Zhong N, Yao L, et al. Mechanisms of shale gas storage: Implications for shale gas exploration in China. AAPG Bull. 2013;97(8):1325–46.
[10] Dai JX, Zou CN, Dong DZ, Ni YY, Wu W, Gong DY, et al. Geochemical characteristics of marine and terrestrial shale gas in China. Mar Petrol Geol. 2016;76:444–63.
[11] Wang SQ, Chen GS, Dong DZ, Yang G, Lu ZG, Xu YH, et al. Accumulation conditions and exploitation prospect of shale gas in the lower Paleozoic Sichuan Basin. Nat Gas Ind. 2009;29:51–8.
[12] Xu QL, Liu B, Ma YS, Song XM, Wang YJ, Xin XK, et al. Controlling factors and dynamical formation models of lacustrine organic matter accumulation for the Jurassic Da'anzhai Member in the central Sichuan Basin, southwestern China. Mar Petrol Geol. 2017;86:1391–405.
[13] Jarvie DM. Shale resource systems for oil and gas: part 1-shale gas resource systems. AAPG Memoir. 2012;97:89–119.

[14] Jarvie DM. Geochemical assessment of unconventional shale gas resource systems. Fundamentals of gas shale reservoirs. 2015;47–69.
[15] Guo TL, Liu RB. Implications from marine shale gas exploration breakthrough in complicated structural area at high thermal stage: taking Longmaxi Formation in Well JY1 as an example. J Nat Gas Sci Eng. 2013;24(4):643–51.
[16] Huang JL, Zou CN, Li JZ, Dong DZ, Wang SJ, Wang SQ, et al. Shale gas generation and potential of the Lower Cambrian Qiongzhusi Formation in Southern Sichuan Basin, China. Pet Exp Dev. 2012;39(1):69–75.
[17] Guo TL, Zhang HR. Formation and enrichment mode of Jiaoshiba shale gas field, Sichuan Basin. Pet Exp Dev. 2014;1:28–34.
[18] He ZL, Nie HK, Zhang YY. The main factors of shale gas enrichment of Ordovician Wufeng Formatiom – Silurian Longmaxi Formation in the Sichuan Basin and its adjacent areas. Front Earth Sci-Pre. 2016;23(2):8–17.
[19] Dai JX, Ni YY, Gong DY, Feng ZQ, Liu D, Peng WL, et al. Geochemical characteristics of gases from the largest tight sand gas field (sulige) and shale gas field (fuling) in china. Mar Petrol Geol. 2016;79:426–38.
[20] Chen SB, Zhu YM, Chen S, Han YF, Fu CQ, Fang JH. Hydrocarbon generation and shale gas accumulation in the longmaxi formation, southern sichuan basin, china. Mar Petrol Geol. 2017;86:248–58.
[21] Liu Y, Zhang JC, Zhang P, Liu ZY, Zhao PW, Huang H, et al. Origin and enrichment factors of natural gas from the Lower Silurian Songkan Formation in Northern Guizhou Province, South China. Int J Coal Geol. 2018;187:20–9.
[22] Guo RB, Zhang JC, Zhao PW, Tang X, Liu ZY. Accumulation conditions and an analysis of the origins of natural gas in the Lower Silurian Shiniulan Formation from Well Anye 1, Northern Guizhou Province. Energies. 2019
[23] Wang ZH, Tan QY, He L, Cheng JX, Wang RH. Deposition and sequence stratigraphy of the Silurian Shiniulan Formation in southeastern Sichuan-northern Guizhou Province. Oil Gas Geol. 2013;34(4):499–507.
[24] Wang RH, Tan QY, Fu JY, Cheng JX, Wang ZH, He L, et al. Sedimentary characteristics of the Silurian organic reefs from the Shiniulan Formation in southeastern Sichuan. Sediment Geol Tethyan Geol. 2013;2:12–8.
[25] Rong JY, Chen X, Su YZ, Ni YN, Zhan RB, Chen TE, et al. Silurian paleogeography of China. In: Landing E, Johnson ME, editors. Silurian lands and seas-paleogeography outside of Laurentia. New York State Mus Bull. 2003;493:243–98.
[26] Wen L, Hu SY, Tian HQ. A study on hydrocarbon source rock of Cambrian in Yangtze area, China. NW Geol. 2001;34:67–74 (in Chinese with English abstract).
[27] Regional geology of Guizhou Province. Beijing: Geological Publishing House; 1987.
[28] Tang X, Zhang JC, Jiang ZX, Zhang RF, Lan CL, Zhao WS, et al. Heterogeneity of organic-rich lacustrine marlstone succession and their controls to petroleum expulsion, retention, and migration: a case study in the Shulu Sag, Bohai Bay Basin, China. Marine and Petroleum Geology; 2018;96:166–78.
[29] Yang C, Zhang JC, Wang XZ, Tang X, Chen YC, Jiang LL, et al. Nanoscale pore structure and fractal characteristics of marine-continental transitional shale: a case study from the lower permian Shanxi shale in the southeastern ordos basin, china. Mar Petrol Geol. 2017; 88.
[30] Ding JH, Zhang JC, Tang X, Huo ZP, Han SB, Lang Y, et al. Elemental geochemical evidence for depositional conditions and organic matter enrichment of black rock series strata in an inter-platform basin: the lower carboniferous datang formation, Southern Guizhou, Southwest China. Minerals. 2018;8:11.
[31] Chen X, Rong JY. Telychian stage of landdovery series of Yangtze Region China. Beijing: Science Press; 1996.
[32] Ni C, Li Y, Yu SY. From near-shore to off-shore: facies differentiation of the Upper SongKan Menber (Shiniulan,Silurian) in the Northern Guizhou Province, China. Acta Micropalaeontol Sin. 2015;32(4):430–7.
[33] Rong JY, Chen X, Wang Y, Zhan RB, Liu JB, Huang B, et al. Northward expansion of Central Guizhou Oldland through the Ordovician and Silurian transition: evidence and implications (in Chinese). Sci Sin Terrae. 2011;40(10):1407–15.
[34] Rong JY, Chen X, Wang CY, Geng LY, Wu HJ, Deng ZQ, et al. Some problems concerning the correlation of the Silurian rocks in South China. J Stratigr. 1990;3:161–77.
[35] Lin BY, Su YZ, Zhu XF, Rong JY. Chinese stratigraphic code – Silurian. Beijing: Geological Publishing House; 1998.
[36] Gong LZ. Divisions, correlations and unified names of Silurian rock Stratigraphies in Northern and Southeastern Guizhou. Guizhou Geo. 1990;4:33–43.
[37] Gale JFW. Natural fractures in the Barnett Shale and their important for hydraulic fracture treatment. AAPG Bull. 2007;91(4):603–22.
[38] Li XJ, Hu SY, Cheng KM. Suggestions from the development of fractured shale gas in North America. Pet Exp Dev. 2007;34(4):13–21.
[39] Curtis JB. Fractured shale-gas systems. AAPG Bull. 2002;86(11):1921–38.
[40] Jarvie D. Evaluation of hydrocarbon generation and storage in the Bamett Shale, Ft. Worth basin, Texas. Texas: Humble Geochemical Services Division; 2004.
[41] Wang X, Liu YH, Zhang M, Hu SY, Liu HJ. Conditions of formation and accumulation for Shale gas. Nat Gas Ind. 2010;02:180–6.
[42] Ding WL, Li C, Li CY, Xu CC, Jiu K, Zeng WT. Dominant factor of fracture development in shale and its relationship to gas accumulation. Front Earth Sci-Pre. 2012;019(002):212–20.
[43] Nelson SR. Fractionation of heavy hydrocarbon process material. US, US4502944 A[P]; 1985.
[44] Sondergeld CH, Ambrose RJ, Rai CS, Moncrieff J. Micro-structural studies of gas shales. SPE unconventional gas conference. Pittsburgh, Pennsylvania, USA: Society of Petroleum Engineers; 2010.
[45] Ross DJK, Bustin RM. Characterizing the shale gas resource potential of Devonian- Mississippian strata in the Western Canada sedimentary basin: application of an integrated formation evaluation. AAPG Bull. 2008;92(1):87–125.
[46] Ambrose RJ. Micro-structure of gas shales and its effects on gas storage and production performance. Doctoral Dissertations, The University of Oklahoma; 2011.
[47] Schettler JPD, Parmely CR. Contributions to total storage capacity in Devonian shales. SPE Eastern Regional Meeting. Kentucky: Society of Petroleum Engineers; 1991.
[48] Ross DJK, Marc, Bustin R. The importance of shale composition and pore structure upon gas storage potential of shale gas reservoirs. Mar Petrol Geol. 2009;26(6):916–27.

[49] Schieber J. Common themes in the formation and preservation of intrinsic porosity in shales and mudstones-illustrated with examples across the Phanerozoic. SPE Unconventional Gas Conference. Pittsburgh, Pennsylvania, USA: Society of Petroleum Engineers; 2010.
[50] Loucks RG, Reed RM, Ruppel SC, Hammes U, Ma C, Dong C, et al. Spectrum of pore types and networks in mudrocks and a descriptive classification for matrix-related mudrock pores. AAPG Bull. 2012;96(6):1071–98.
[51] Doughty PT. Clay smear seals and fault sealing potential of an exhumed growth fault, Rio Grande rift, New Mexico. AAPG Bull. 2003;87(3):427–44.
[52] Smith DA. Theoretical consideration of sealing and nonsealing faults. AAPG Bull. 1966;50:363–74.
[53] Ingram GM, Urai JL. Top-seal leakage through faults and fractures: the role of mudrock properties. Geol Soc. 1999;158(1):125–35.
[54] Schlömer S, Krooss BM. Experimental characterisation of the hydrocarbon sealing efficiency of cap rocks. Mar Petrol Geol. 1997;14(5):565–80.
[55] Donald LZ. Hydrocarbon columns, buoyancy pressures, and seal efficiency; comparisons of oil and gas accumulations in California and the Rocky Mountain area. AAPG Bull. 1992;76(4):501–8.
[56] Marlan WD. Evaluating seals for hydrocarbon accumulations. AAPG Bull. 1984;68(11):1752–63.
[57] Liu B, Yang Y, Li J, Chi Y, Li J, Fu X. Stress sensitivity of tight reservoirs and its effect on oil saturation: a case study of Lower Cretaceous tight clastic reservoirs in the Hailar Basin, Northeast China. J Petrol Sci Eng. 2020;184:106484.
[58] Liu B, Song Y, Zhu K, Su P, Ye X, Zhao W. Mineralogy and element geochemistry of salinized lacustrine organic-rich shale in the middle Permian Santanghu Basin: implications for paleoenvironment, provenance, tectonic setting and shale oil potential. Marine Petrol Geol. 2020;120:104569.
[59] Pang F, Bao SJ, Zhai GY. Major breakthroughs in oil and gas in Anye-1 Well in Wulingshan structural area. Manag Res Sci Technol Achiev. 2016;49–50.
[60] Yuan YS, Zhou Y, Qiu DF, Wang XX. Formation mechanism and characteristic of non-tectonic fractures in shale. Geoscience. 2016;30(1):155–62.
[61] Wang R, Hu Z, Liu J, Wang X, Gong D, Yang T. Comparative analysis of characteristics and controlling factors of fractures in marine and continental shales: a case study of the Lower Cambrian in Cengong area, Northern Guizhou Province. Oil Gas Geol. 2018;39(4):631–40.
[62] Wang R, Nie H, Hu Z, Liu G, Xi B, Liu W. Controlling effect of pressure evolution on shale gas reservoirs: a case study of the Wufeng–Longmaxi Formation in the Sichuan Basin. Nat Gas Ind. 2020;40(10):1–11.
[63] Zhao K, Du P. A new production prediction model for multi-stage fractured horizontal well in tight oil reservoirs. Adv Geo-Energy Res. 2020;4(2):152–61. doi: 10.26804/ager.2020.02.04.
[64] Zhang G, Zhang Y, Xu A, Li Y. Microflow effects on the hydraulic aperture of single rough fractures. Adv Geo-Energy Res. 2019;3(1):104–14. doi: 10.26804/ager.2019.01.09.
[65] Gou Q, Xu S. Quantitative evaluation of free gas and adsorbed gas content of Wufeng-Longmaxi shales in the Jiaoshiba area, Sichuan Basin, China. Adv Geo-Energy Res. 2019;3(3):258–67. doi: 10.26804/ager.2019.03.04.
[66] Anders MH, Laubach SE, Scholz CH. Microfractures: a review. J Struct Geol. 2014;69:377–94.
[67] Liu J, Ding W, Xiao Z, Dai J. Advances in comprehensive characterization and prediction of reservoir fractures. Prog Geophys. 2019;34(6):2283–300.